THE JOURNAL OF BIOLOGICAL CHEMISTRY
Vol. 280, No. 5, Issue of February 4, pp. 3928–3937, 2005
Printed in U.S.A.

Macromolecular Accessibility of Fluorescent Taxoids Bound at a Paclitaxel Binding Site in the Microtubule Surface*

Received for publication, July 12, 2004, and in revised form, November 5, 2004
Published, JBC Papers in Press, November 18, 2004, DOI 10.1074/jbc.M407816200

José Fernando Díaz‡§, Isabel Barasoain‡, André A. Souto¶‖, Francisco Amat-Guerri¶, and José Manuel Andreu‡

From the ‡Centro de Investigaciones Biológicas, Consejo Superior de Investigaciones Científicas, Ramiro de Maeztu 9, Madrid 28040 and the ¶Instituto de Química Orgánica, Consejo Superior de Investigaciones Científicas, Juan de la Cierva 3, Madrid 28006, Spain

The macromolecular accessibility of the paclitaxel binding site in microtubules has been investigated using a fluorescent taxoid and antibodies against fluorescein, which cannot diffuse into the microtubule lumen. The formation of a specific ternary complex of microtubules, Hexaflutax (7-*O*-{*N*-[6-(fluorescein-4′-carboxamido)-*n*-hexanoyl]-L-alanyl}paclitaxel) and 4-4-20 IgG (a monoclonal antibody against fluorescein) has been observed by means of sedimentation and electron microscopy methods. The kinetics of binding of the antibody to microtubule-bound Hexaflutax has been measured. The quenching of the observed fluorescence is fast (k_+ 2.26 ± 0.25 × 10^6 M^{-1} s^{-1} at 37 °C), indicating that the fluorescein groups of Hexaflutax are exposed to the outer solvent. The velocity of the reaction is linearly dependent on the antibody concentration, indicating that a bimolecular reaction is being observed. Another fluorescent taxoid (Flutax-2) bound to microtubules has also been shown to be rapidly accessible to polyclonal antibodies directed against fluorescein. A reduced rate of Hexaflutax quenching by the antibody is observed in microtubule-associated proteins containing microtubules or in native cellular cytoskeletons. It can be concluded that the fluorescent taxoids bind to an outer site on the microtubules that is shared with paclitaxel. Paclitaxel would be internalized in a further step of binding to reach the known luminal site, this step being blocked in the case of the fluorescent taxoids. Because the fluorescent ligands are able to induce microtubule assembly, binding to the outer site should be enough to induce assembly by a preferential binding mechanism.

The paclitaxel (Taxol®, Bristol-Myers Squibb) binding site of microtubules (1, 2) is emerging as a ubiquitous target for substances extracted from many types of different organisms, including prokaryotes (epothilones from *Sorangium cellulosum*) (3) and eukaryotes, both vegetal (paclitaxel from yew) (4) and animal (discodermolide from sea sponges and eleutherobin from coral) (5, 6). These compounds, called microtubule-stabilizing agents, bind to microtubules, stabilize them, and block their dynamics, thus disrupting cell division. Subsequently, because they block cell division they are useful as antitumor drugs. Paclitaxel and its derivatives are the main choices for the chemotherapy of ovarian cancer, metastatic breast cancer, head and neck cancer, and lung cancer (7).

The location of the paclitaxel binding site of microtubules has been the object of research for a decade. Early low resolution microtubule models placed the paclitaxel binding site in between the protofilaments of microtubules (8). A compatible location was observed in the projection difference map of zinc-induced tubulin sheets at 6.5 Å resolution (9). This location of the binding site would have been compatible with the currently established facts that taxoids are able to access their binding site very rapidly (10–12) and that taxoids do not bind to unassembled tubulin (13) (which suggests that the interprotofilament contact might be necessary for the existence of the binding site).

The quest for the location of the binding site got a first answer from the atomic structure of tubulin. Tubulin had been an elusive protein for high resolution structural studies; its inhomogeneity and instability precluded the determination of its three-dimensional structure until the late nineties. In the brilliant study of Nogales *et al.* (14), the structure of tubulin was solved by electron crystallography of paclitaxel-stabilized zinc-induced tubulin sheets, a polymer of tubulin whose topology is different from that of microtubules (15). Although both microtubules and zinc sheets are composed of protofilaments that consist of tubulin dimers aligned head to tail, in the case of microtubules, protofilaments associate laterally and close to give a cylinder whose number of protofilaments ranges from 11 to 16 (8, 16, 17). In the case of the zinc-induced sheets, protofilaments associate in an antiparallel way, resulting in a flat sheet that is suitable for two-dimensional electron crystallography (9).

The protofilament structure directly determined from the zinc-induced sheets was fitted into electron microscopy density maps of microtubules (18, 19) to obtain pseudo-atomic resolution maps of microtubules (19–21). The constructed models are supported by the 8 Å three-dimensional reconstruction of microtubules from cryoelectron microscopy (22). Because the zinc-induced sheets employed included paclitaxel as stabilizer, the location of the paclitaxel binding in the microtubules was thus known. Surprisingly, the translation of the zinc sheet protofilaments into microtubules results in a paclitaxel binding site inside the lumen of the tube, hidden from the outer solvent (20).

The kinetics of binding of several taxoids (including paclitaxel) to their site in the microtubules was subsequently determined (11, 12). The association rate constant of paclitaxel to

* This work was supported by Grants BIO 2001-1725 from Ministero de Ciencia y Tecnología (to J. F. D.), 07B/0026/2002 from Comunidad Autonoma de Madrid (to J. M. A.), and BQU2000-1500 (to F. A.-G.). The costs of publication of this article were defrayed in part by the payment of page charges. This article must therefore be hereby marked "*advertisement*" in accordance with 18 U.S.C. Section 1734 solely to indicate this fact.

This paper is dedicated to the memory of Dr. José Laynez, who provided support and encouragement during this work.

§ To whom correspondence should be addressed. Tel.: 34-918-373-112 (ext. 4380); Fax: 34-915-360-432; E-mail: fer@cib.csic.es.

‖ Present address: Faculdade de Química, Universidade Pontificia Catolica do Rio Grande do Sul, 90619-900, Porto Alegre-RS, Brazil.

stabilized microtubules assembled from pure tubulin is very high (3.6×10^6 M^{-1} s^{-1}), being an order of magnitude slower for MAP[1]-stabilized microtubules and for native cytoskeletons of PtK2 cells (12). Because a binding site hidden in the microtubule lumen should severely restrict accessibility of the ligands to their target, these results were apparently contradictory with the observed location of the binding site. These kinetic constants are incompatible with any kind of passive diffusion through a pore on the microtubule surface as big as 25 Å diameter (12). The binding reaction of taxoids to microtubules is diffusion-controlled, indicating that the observed binding step is not restricted, and so it corresponds to the binding of the ligand to an exposed site. Because binding is slowed down by a factor of 10 by the presence of MAPs that bind to the microtubule outer surface, the kinetic evidence points to a primary binding site accessible on the microtubule surface.

To reconcile the kinetic data with the structural and biochemical evidence of a paclitaxel binding site placed in the microtubule lumen (20, 23–28), an external initial binding site together with a hypothetical transport mechanism toward the internal binding site have been proposed (12). In this model, taxoids would bind to a putative binding site located in one of the two different types of pores existent in the B-lattice of the microtubules (pore type I, closer to the site in the lumen), being later transported to the luminal site. In this hypothetical mechanism, binding to the external and luminal sites should be mutually exclusive because only 1.0 taxoid molecules bind/tubulin dimer. This could be accomplished if both sites share an element that switches between the two alternative binding sites.

The purpose of this study is to obtain direct evidence of the existence of an external taxoid binding site. To do so, the accessibility of microtubule-bound taxoids to a large macromolecule (an antibody) has been probed, employing fluorescein derivatives of paclitaxel (Flutax-1, Flutax-2, and Hexaflutax) and polyclonal and monoclonal antibodies against the fluorescein moiety. Because it is impossible for a large molecule like an antibody to fit through any realistic pore in the microtubule wall, taxoid molecules bound to the luminal site of the microtubules will be protected from antibodies. Taxoid molecules bound to a site on the surface would react with the antibody, so providing evidence of an exposed taxoid binding site.

In this study, the existence of a specific ternary complex of microtubules, Hexaflutax, and 4-4-20 (a monoclonal antibody against fluorescein) has been observed by means of sedimentation and electron microscopy, providing direct evidence of the existence of an external binding site for the ligand. Further kinetic evidence is given by the kinetics of binding of the antibody to microtubule-bound Hexaflutax, which is fast, indicating that the fluorescein groups of the ligand are homogeneously exposed to the outer solvent. From these results it can be concluded that these fluorescent taxoids bind to an outer site on the microtubules which is shared with paclitaxel.

MATERIALS AND METHODS

Tubulin, Taxoids, and Antibodies—Purified calf brain tubulin and chemicals were as described previously (29). For glycerol-induced assembly, tubulin was equilibrated directly in 10 mM phosphate, 1 mM EGTA, 0.1 mM GTP, 3.4 M glycerol, pH 6.8, buffer. All tubulin samples were clarified by centrifugation at 50,000 rpm, 4 °C, for 10 min using TL100.2 or TL100.4 rotors in Beckman Optima TLX centrifuges. After centrifugation 6 mM $MgCl_2$ and up to 1 mM GTP were added to the solution, final pH 6.5 (glycerol assembly buffer, GAB). Microtubule protein, containing tubulin and MAPs, was prepared in microtubular protein assembly buffer (AB) (100 mM Mes, 1 mM EGTA, 1 mM $MgSO_4$, 2 mM 2-mercaptoethanol, 1 mM GTP, pH 6.5), as described previously (30). Stabilized mildly cross-linked microtubules were prepared as described previously (11, 12, 31). Flutax-1 (7-*O*-[*N*-(fluorescein-4′-carbonyl)-L-alanyl]paclitaxel) and Flutax-2 (7-*O*-[*N*-(2,7-difluorofluorescein-4′-carbonyl)-L-alanyl]paclitaxel) were synthesized as described previously (11, 32). 7-Hexaflutax (7-*O*-{*N*-[6-(fluorescein-4′-carboxamido)-*n*-hexanoyl]-L-alanyl}paclitaxel) was synthesized by the reaction of 5 mg of 7-*O*-[L-alanyl]paclitaxel with a 50% excess of 6-(fluorescein-4′-carboxamido)-n-hexanoic acid succinimidyl ester (Molecular Probes, Eugene, OR) using basically the same procedure. The structures of the ligands are shown in Fig. 1. 7-Hexaflutax was purified by preparative TLC on silica gel with chloroform/hexane/methanol (1:1:0.2, v/v/v) as eluent. Yield, 4.13 mg, 55%; 1H RMN (400 MHz, $CDCl_3$, room temperature) (see numbering (32)): 8.89 (m, 3H, H-5′F, *o*-H-Ph(a)), 8.25 (s, 1H, H-3′F), 7.67 (d, 2H, *o*-H-Ph(c)), 7.52–7.05 (m, 12H, H-6′F, *m*-, *p*-H-Ph(a), *o*-, *m*-, *p*-H-Ph(b), *m*-, *p*-H-Ph(c)), 6.70 (d, 2H, H-2F, H-7F), 6.49 (s, 2H, H-4F, H-5F), 6.42 (d, 2H, H-1F, H-8F), 6.13 (s, 1H, H-10), 5.95 (t, 1H, H-13), 5.34–5.48 (m, 3H, H-2, H-7, H-3′), 4.85 (d, 1H, H-5), 4.54 (d, 1H, H-2′), 4.12 (q, 1H, CH-Ala), 3.99 (m, 2H, H-20), 3.70 (d, 1H, H-3), 3.42 (q, 2H, CH_2NH), 3.26 (t, 2H, CH_2CO), 2.26 (m, 1H, H-6a), 2.15 (s, 3H, 4-CH_3CO), 2.08 (m, 2H, H-14), 1.97 (s, 3H, 10-CH_3CO), 1.79 (s, 3H, H-18), 1.60 (m, 1H, H-6b), 1.59 (s, 3H, H-19), 1.40–1.50 (m, 4H, 2×CH_2), 1.08 (d, 3H, CH_3-Ala), 0.97 (s, 3H, H-17), 0.93 (s, 3H, H-16) ppm. Electrospray ionization mass spectrometry (positive mode): 1,396.3 [MH+]. Hexaflutax purity was 97.7% (high performance liquid chromatography (10)). Taxoids were dissolved in dimethyl sulfoxide, and their concentrations were measured spectrophotometrically as described previously (10, 12, 29) except for the Hexaflutax concentration, which was measured in 0.5% SDS, 50 mM sodium phosphate buffer, pH 7.0, employing an extinction coefficient of ϵ_{458} 24,200 ± 600 M^{-1}. The solubility of Hexaflutax in GAB in the absence of tubulin was found to be of the order of 10 μM. Docetaxel (Taxotere®); was kindly provided by Rhône-Poulenc Rorer (Antony, France). Antifluorescein polyclonal rabbit IgG and 4-4-20 antifluorescein monoclonal mouse IgG (33) were gifts from Prof. Edward W. Voss Jr. (University of Illinois at Urbana-Champaign). They were concentrated by precipitation with 50% ammonium sulfate, centrifuged for 25 min at 19,000 rpm in a SS-34 rotor employing a Sorvall RC-5B centrifuge, and the pellets were resuspended in 10 mM phosphate and 150 mM NaCl, pH 7.0. The remaining ammonium sulfate was eliminated with a gel filtration chromatography (HiTrap desalting, Amersham Biosciences) in the same buffer, and finally the antibodies were concentrated using Centricon 10 concentrators (Amicon, Bedford, MA) and kept at −80 °C until used. Prior to the measurements the concentration of sites in the polyclonal antibody was carefully titrated with fluorescein, Flutax-1, Flutax-2, and Hexaflutax, 20% of the total IgG was found to be active against fluorescein. The IgG fraction of a nonimmune rabbit serum was purified as described previously (34) and concentrated as the other IgGs. P11E12 (anti-β-tubulin N-terminal) and P12E11 (anti-α-tubulin C-terminal) mouse monoclonal IgGs were obtained as described previously (35–37). MOPC 21-purified mouse IgG was from Sigma.

Cosedimentation Assay of Ternary Complex Formation—10 μM GTP-tubulin in PEDTA 7 GTP buffer (10 mM sodium phosphate, 1 mM EDTA, 7 mM $MgCl_2$, 1 mM GTP, pH 6.7) in the presence of 12 μM Hexaflutax was incubated at 37 °C for 30 min, in the presence or absence of 12 μM 4-4-20 monoclonal antibody and 100 μM docetaxel; alternatively, 4 μM paclitaxel binding sites in preassembled cross-linked microtubules (4.5 μM) in GAB were incubated for 1 min at 25 °C with the desired reactives. The samples were immediately centrifuged for 20 min at 50,000 rpm in a TLA 100 rotor, employing a Beckman Optima TLX ultracentrifuge. The supernatants were taken and the pellets carefully resuspended in 10 mM sodium phosphate, 1% SDS, pH 7.0, buffer. An aliquot of supernatants and pellets was diluted 1/5 in 10 mM sodium phosphate, 1% SDS, pH 7.0, buffer and incubated for 15 min at 80 °C to dissociate the antibody-fluorescein complex. The fluorescence of the samples was measured in a Shimadzu RF-540 spectrofluorometer employing λ_{exc} 495, λ_{ems} 520 nm, 5 nm excitation and emission slits, to quantify the amount of ligand in supernatant and pellets. The supernatants and pellets were also diluted 1/2 in electrophoresis sample buffer, and the presence of antibodies in them was assayed with a nonreducing SDS-PAGE in 7.5% acrylamide gel.

Electron Microscopy of the Ternary Complex—A mixture of 4 μM sites in cross-linked microtubules, 2 μM Hexaflutax, and 2 μM 4-4-20 antibody was adsorbed for 1 min to a copper grid covered with formvar and

[1] The abbreviations used are: MAP, microtubule-associated protein; AB, microtubular protein assembly buffer, GAB, glycerol assembly buffer; Mes, 4-morpholineethanesulfonic acid; Pipes, 1,4-piperazinediethanesulfonic acid; paclitaxel, 4,10-diacetoxy-2a-(benzoyloxy)-5b,20-epoxy-1,7b-dihydroxy-9-oxotax-11-en-13a-yl(2*R*,3*S*)-3-[(phenylcarbonyl)-amino]-2-hydroxy-3-phenylpropionate); docetaxel, 4-acetoxy-2a-(benzoyloxy)-5b,20-epoxy-1,7b,10b-trihydroxy-9-oxotax-11-en-13a-yl(2*R*,3*S*)-3-[(*tert*-butoxycarbonyl)amino]-2-hydroxy-3-phenylpropionate).

carbon. The grids were blotted and then incubated over a drop of GAM-10, a nanogold-labeled goat anti-mouse antibody (British Biocell International, Cardiff, UK), for 5 min. The grids were then washed with 5 drops of GAB and stained for 2 min with 2% uranyl acetate in water. The grids were observed in a JEOL JEM-1200-EXII microscope.

Fluorescence Spectroscopy and Anisotropy Measurements—Corrected fluorescence spectra were acquired with a photon counting Fluorolog-3–221 instrument (Jobin Yvon-Spex, Longiumeau, France), employing 1 nm excitation and 5 nm emission bandwidths, at 25 °C. Fluorometric concentration measurements were made with a Shimadzu RF-540 spectrofluorometer. Anisotropy values were collected in the Fluorolog T-format mode with vertically polarized excitation and corrected for the sensitivity of each channel with horizontally polarized excitation (38).

Binding of Taxoids to Microtubules—Binding constants of Hexaflutax to microtubules were obtained using anisotropy titration measurements. 200 nM Hexaflutax in GAB was incubated for 30 min with increasing concentrations of binding sites in stabilized cross-linked microtubules (from 0 to 10 μM) at the desired temperature, and the anisotropy of the solution was measured in a POLARSTAR BMG plate reader in the polarization mode, employing the 480-P excitation filter and the 520-P emission filters (38). Alternatively, the binding constants of Hexaflutax and the 4-4-20-Hexaflutax complex were measured using a centrifugation assay. Samples of 1 μM taxoid binding sites in cross-linked microtubules were incubated for 30 min at 25 °C with different concentrations of Hexaflutax in the presence and absence of antibody. The samples were centrifuged for 20 min at 50,000 rpm in a TL100 rotor employing a Beckman TLX ultracentrifuge. The pellets and supernatants were diluted 1/5 in 10 mM sodium phosphate, pH 7.0, 1% SDS and warmed up at 95 °C for 3 min to dissociate the Hexaflutax-antibody complex and their fluorescence measured employing a Shimadzu RF-540 spectrofluorometer (excitation wavelength 495 nm, emission wavelength 527 nm, 5 nm excitation and emission slits). The concentration of ligand in the samples was calculated using Hexaflutax spectrophotometric concentration standards.

Kinetics of Binding of Antibodies to Microtubules—The fast kinetics of binding of the 4-4-20 antibody to Hexaflutax bound to stabilized microtubules or free in solution was measured by the change of intensity of fluorescence using a Bio-Logic SF300S stopped flow device equipped with a fluorescence detection system with an excitation wavelength of 484 nm and a filter with a cutoff of 520 nm in the emission pathway. The fast kinetics of binding of the anti-fluorescein polyclonal IgG to Flutax-1, Flutax-2 bound to stabilized microtubules, was measured by the change of intensity of fluorescence using a High-Tech Scientific SS-51 stopped flow device equipped with a fluorescence detection system using an excitation wavelength of 492 nm and a filter with a cutoff of 530 nm in the emission pathway. The slow kinetics of binding of 4-4-20 antibody to Hexaflutax bound to MAPs containing microtubules was measured with a photon counting instrument Fluorolog-3-221 (Jobin Yvon-Spex, Longiumeau, France) with an excitation wavelength of 495 nm (0.1 nm band pass to prevent photolysis) and an emission wavelength 525 nm (5 nm band pass). The fitting of the kinetic curves was done with a nonlinear least squares fitting program based on the Marquardt algorithm (39); additionally the FITSIM package (40) was employed for the data shown in Fig. 4*B*.

Cytoskeletons and Fluorescence Microscopy—PtK2 potoroo epithelial like kidney cells were grown as described previously (41). Coverslip-attached PtK2 cytoskeletons were obtained as described before (12). The cytoskeletons were dipped into 3 μM Hexaflutax for 2 min, then they were washed eight times with 2 ml of PEMP (100 mM Pipes, 1 mM EGTA, 1 mM $MgCl_2$, 4% polyethylene glycol, pH 6.8), changing the washing well after four washes, then incubated with either PEMP, 0.2 or 1 μM antifluorescein 4-4-20 monoclonal antibody for different times, washed again eight times as above, and mounted with 20 μl of PEMP, and their images were recorded with a Zeiss Axioplan epifluorescence microscope using a 100× Plan-Apochromat objective and a Hamamatsu 4742–95 cooled CCD camera (42). In other experiments cytoskeletons were dipped into either 1 μM Flutax-1 or 1 μM Flutax-2 for 5 min, washed eight times as above, incubated with either 0.2 or 1 μM antifluorescein monoclonal antibody or 1 or 5 μM polyclonal anti-fluorescein IgG for different times, and washed and visualized as above. Antifluorescein antibodies preincubated with fluorescein were used as controls in which quenching was inhibited. The fluorescence intensities of a minimum of 40 different fields/time point were integrated using Sigma Scan 5.0 (SPSS Inc., Chicago) and averaged.

Molecular Modeling—The complexes between the 4-4-20 Fab fragment, Hexaflutax, and the microtubules were modeled by placing the ligands in the paclitaxel binding site of microtubules constructed using the model of Chacón and Wriggers (21). The 4-4-20 Fab fragment was placed in its place by replacing the fluorescein molecule of the 1FLR PDB entry (43) by the fluorescein moiety of 7-Hexaflutax. The bonds of the linker between both moieties were rotated to expose the fluorescein moiety to the outer solvent via the type 1 pores (12) (for the case of the Hexaflutax-microtubule complex) and to minimize the steric hindrances between the Fab and tubulin (for the case of the 4-4-20-Hexaflutax-microtubule complex).

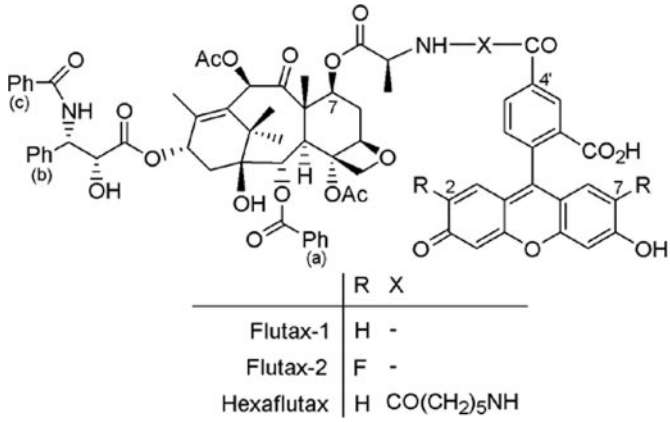

FIG. 1. **Structures of Flutax-1, Flutax-2, and Hexaflutax.**

RESULTS

Binding of Fluorescent Taxoids to Microtubules and to Antibodies—The structures of the fluorescent taxoids employed in this study are shown in Fig. 1. The spectroscopy properties of free and microtubule-bound Hexaflutax were characterized in the different buffers employed in the study. Upon binding to microtubules, Hexaflutax undergoes a 40% reduction in its fluorescence intensity at 527 nm (λ_{exc} 495), no displacements of the emission or excitation maxima being observed. The anisotropy of the fluorescence increases from 0.06 to 0.18 upon binding, independently from the buffer employed.

The interaction of Hexaflutax with the paclitaxel site was characterized using sedimentation and fluorescence techniques. Hexaflutax binds to the paclitaxel binding site of microtubules, although with 60 times lower affinity than Flutax-1 and Flutax-2 (K_a Hexaflutax, 27 °C $9.6 \pm 1.12 \times 10^5$ M^{-1}; K_a Flutax-1, 27 °C $6.0 \pm 0.2 \times 10^7$ M^{-1}; K_a Flutax-2, 27 °C $5.9 \pm 0.3 \times 10^7$ M^{-1} (11) (fluorescence anisotropy data)), being displaced from the binding site by an excess of docetaxel (a closely related ligand with a higher solubility than paclitaxel). At the maximum free soluble concentration of Hexaflutax (~10 μM) 1 μM binding sites in cross-linked microtubules bind stoichiometric amounts of the ligand, indicating only one high affinity binding site. From the above data it can be said that Hexaflutax is a *bona fide* probe of the paclitaxel binding site, as is the case for Flutax-1 and Flutax-2 (11, 12).

The capability of the antibodies employed (a monoclonal IgG (4-4-20 (33)) and a polyclonal IgG against fluorescein) to bind Flutax-1, Flutax-2, and Hexaflutax was characterized by measuring both the quenching of the fluorescence of the ligand and the increase in the anisotropy caused by its immobilization upon binding to the antibody. Although the polyclonal IgG is able to quench completely the fluorescence of the ligands, the monoclonal 4-4-20 antibody only does it partially (Flutax-1, 55% quenching; Flutax-2, 65% quenching; Hexaflutax, 80% quenching; Hexaflutax-microtubule complex, 77% quenching (86% if compared with the free Hexaflutax fluorescence)), probably because the paclitaxel moiety may interfere with the formation of the fluorescein-4-4-20 antibody complex. Additionally, although 1 μM 4-4-20 quenches almost completely (more than 90% of the maximum observed quenching) 100 nM Hexaflutax, high concentrations of 4-4-20 (more than 5 μM for 100 nM Flutax-1 or Flutax-2) are needed to obtain 50% of the maximum observed quenching, which indicates low affinity of

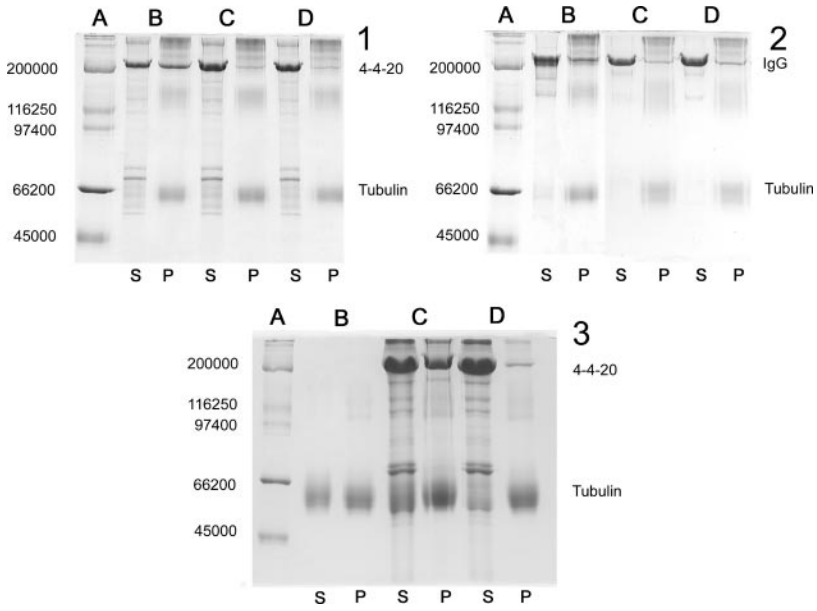

FIG. 2. **Sedimentation assay of antibody binding to microtubules.** *Gel 1. Lane A*, high molecular weight standards (Bio-Rad); *lanes B–D*, Coomassie-stained nonreducing SDS gels (7.5%) of the supernatants (*S*) and pellets (*P*) of the centrifugation of the following reaction mixtures in GAB: *lane B*, 4.5 μM stabilized microtubules (4 μM sites), 2 μM Hexaflutax, 2 μM 4-4-20 antibody; *lane C*, 4.5 μM stabilized microtubules (4 μM sites), 2 μM Hexaflutax, 2 μM 4-4-20 antibody, 100 μM docetaxel; *lane D*, 4.5 μM stabilized microtubules (4 μM sites), 2 μM Hexaflutax, 2 μM 4-4-20 antibody, 50 μM fluorescein. *Gel 2*. *Lane A*, high molecular weight standards (Bio-Rad); *lanes B–E*, Coomassie-stained nonreducing SDS gels (7.5%) of the supernatants and pellets of the centrifugation of the following mixtures in GAB: *lane B*, 4.5 μM stabilized microtubules (4 μM sites), 2 μM P12E11 monoclonal mouse antibody anti-α-tubulin-C-terminal; *lane C*, 4.5 μM stabilized microtubules (4 μM sites), 2 μM P14B4 monoclonal mouse antibody anti-β-N-terminal; *lane D*, 4.5 μM microtubules (4 μM sites), 2 μM mouse myeloma IgG MOPC 21 (Sigma). *Gel 3. Lane A*, high molecular weight standards (Bio-Rad); *lanes B–D*, Coomassie-stained nonreducing SDS gels (7.5%) of the supernatants and pellets of the centrifugation of the following mixtures in PEDTA 7 GTP: *lane B*, 10 μM GTP-tubulin, 12 μM Hexaflutax; *lane C*, 10 μM GTP-tubulin, 12 μM Hexaflutax, 12 μM 4-4-20 antibody; *lane D*, 10 μM GTP-tubulin, 12 μM Hexaflutax, 12 μM 4-4-20 antibody, 100 μM docetaxel.

the antibody for these two ligands. The ligands show a large increase of the anisotropy of the fluorescence upon binding to the antibodies (Flutax-1 free, 0.05; bound, 0.25; Flutax-2 free, 0.05; bound, 0.25; Hexaflutax free, 0.06; bound, 0.18).

Binding of Antibodies to Fluorescent Taxoids Bound to Microtubules—To measure directly the accessibility of fluorescent taxoids bound to microtubules to an antibody, cosedimentation experiments were performed. It was not possible to isolate a ternary complex between Flutax-1 or Flutax-2, microtubules, and antibody. When ligand-bound microtubules were incubated with the antibodies, the ligands dissociated from the microtubules and were found in the supernatant bound to the antibody. Because the linker between the paclitaxel and the fluorescein moiety of Flutax-1 and Flutax-2 (an alanine residue) is very short, and it might compromise the stability of the ternary complex for steric reasons, we used Hexaflutax, a fluorescent taxoid with an additional hexanoyl spacer between the fluorescein and the paclitaxel group.

Fig. 2 (*Gel 1*) shows a nonreducing SDS-PAGE of pellets and supernatants of the cosedimentation experiments performed using Hexaflutax, stabilized microtubules, and 4-4-20 mouse antifluorescein monoclonal antibody. Control measurements showed that in the presence of only microtubules or ligands the antibody is only found in the supernatant (not shown). In the presence of microtubules and ligands (*lanes B*) a significant percentage (45 $\pm$ 5%) of the antibody is present in the pellet, indicating the formation of a ternary complex. It is important to point out that the order in which the reagents are mixed is irrelevant for the result, as would be the case if the preformed 4-4-20-Hexaflutax complex were able to bind fast to the taxoid site in microtubules. If an excess of docetaxel or fluorescein (*lanes C* and *D*) is added to the solution, the antibody is only found in the supernatant (5 $\pm$ 3% of the antibody in the pellet). If the cosedimentation experiment is performed with Flutax-1 or Flutax-2 instead of Hexaflutax, a very faint 4-4-20 band is seen in the pellet for the case of Flutax-1, and no 4-4-20 antibody bound to microtubules is observed when Flutax-2 is employed (not shown). Fig. 2 (*Gel 2*) shows the reactivity of microtubules with other monoclonal mouse IgGs (which are directed against C and N terminus of tubulin) and a control IgG. The P12E11 antibody (against α C-terminal (430–443)) shows a strong reactivity against microtubules (33 $\pm$ 5% of the antibody in the pellet) in agreement with previous results (35). The P14B4 antibody (against β N-terminal (1–13)) shows a weak nonspecific (because this epitope is occluded in the native microtubules) reactivity (8 $\pm$ 5% of the antibody in the pellet). The control MOPC 21 antibody shows a weak nonspecific reactivity as well (10 $\pm$ 3% of the antibody in the pellet). Similar results are obtained employing noncross-linked microtubules that were assembled by Hexaflutax, so they have stoichiometric amounts of the ligand bound (Fig. 2 (*Gel 3*), 42 $\pm$ 5% of the antibody in the pellet in the absence of docetaxel, 7 $\pm$ 5% of the antibody in the pellet in the presence of docetaxel).

When the ternary complex microtubule-Hexaflutax-4-4-20 antibody is incubated with an immunogold-labeled goat anti-mouse antibody, nanogold spheres can been seen associated to the walls of the microtubules (Fig. 3). To confirm the specificity of the binding, the ternary complex was incubated with a large excess of docetaxel prior to the addition of the labeled antibody, and the density of nanogold beads in the presence and absence of docetaxel was quantified. In the absence of docetaxel (Fig. 3*A*) 211 linear μm of microtubules on a 706 μm^2 field were examined, 137 beads were found on the microtubules (0.65 beads/μm), and 84 spheres were found as background (0.12 beads/μm^2). In the presence of 100 μM docetaxel (Fig. 3*B*) 376 linear μm of microtubules in a 1,075 μm^2 field were examined, 41 beads were found bound on microtubules (0.11 beads/μm), and 142 spheres were found as background (0.13 beads/μm^2). Representative micrographs are shown in Fig. 3, *A* and *B*. No

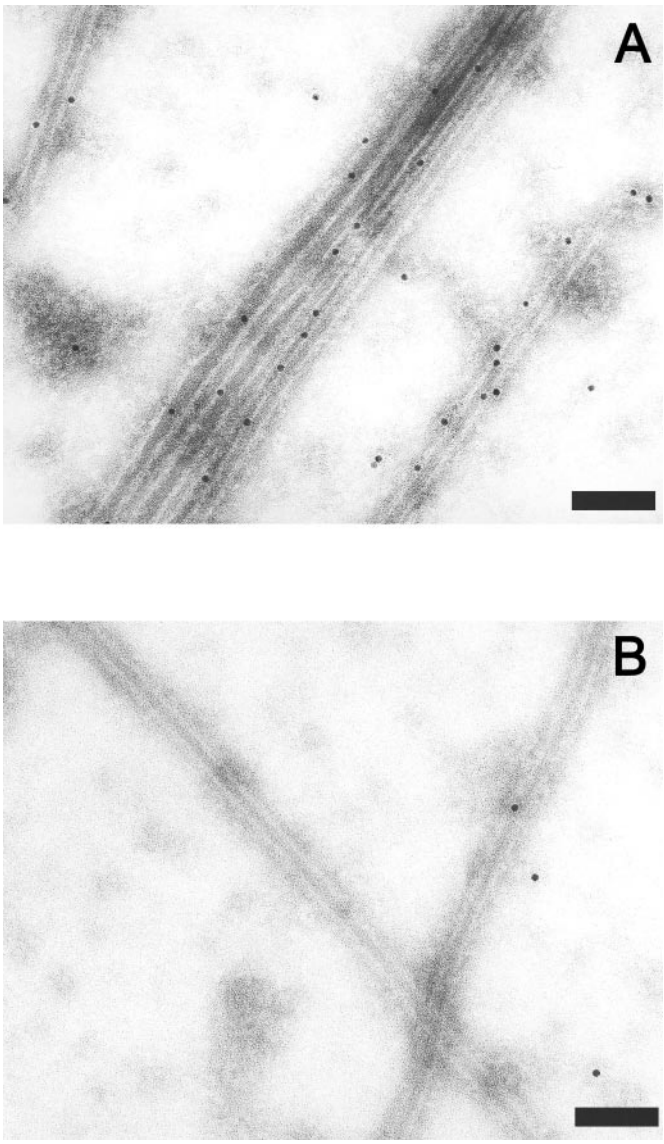

FIG. 3. **Electron micrographs from a solution of stabilized microtubules (4.5 μM tubulin) incubated with immunogold-labeled anti-mouse antibodies in the presence of 2 μM Hexaflutax and 2 μM 4-4-20 antibody (*A*) or 2 μM Hexaflutax, 2 μM 4-4-20 antibody, and 100 μM docetaxel (*B*).** The *bar* represents 100 nm.

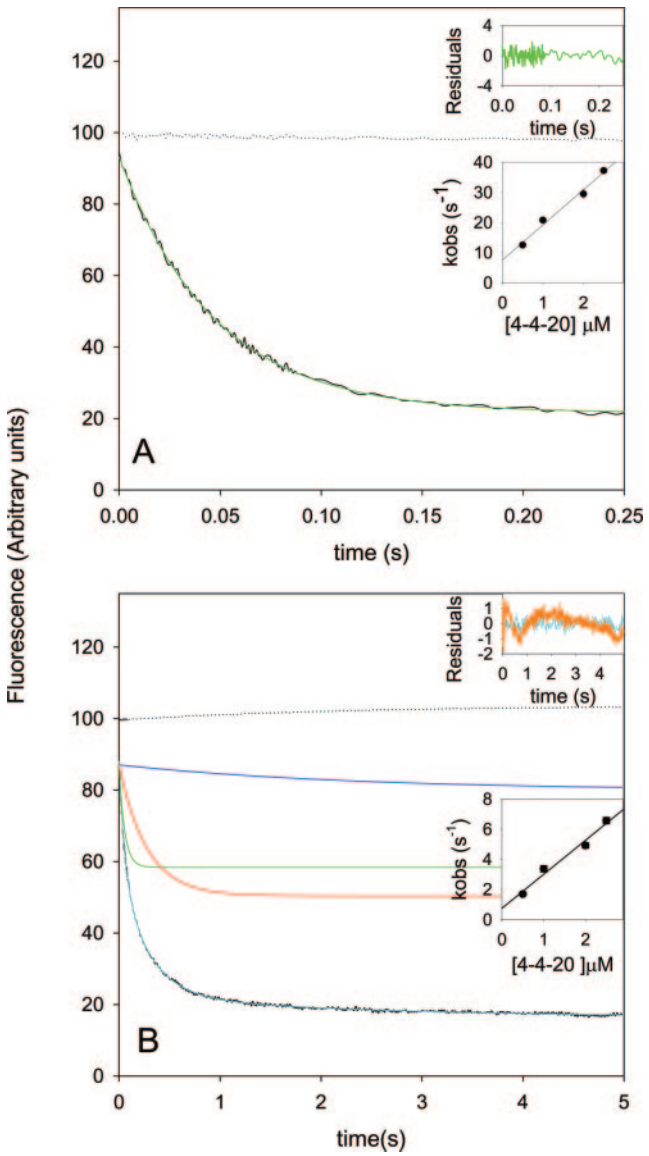

FIG. 4. *A*, kinetics of binding of 4-4-20 IgG to free Hexaflutax at 37 °C. In the stopped flow device a 2 μM solution of 4-4-20 IgG (*solid line*) or GAB (*dotted line*) was mixed with 200 nM Hexaflutax (final concentrations 1 or 0 μM 4-4-20 IgG and 100 nM Hexaflutax); *green line*, fitting of the data to a monoexponential curve. *Upper inset*, residues between the experimental and the fitting curve (*green line*). *Lower inset*, dependence of the observed kinetic rate on the concentration of 4-4-20 IgG. *B*, kinetics of binding of 4-4-20 IgG to Hexaflutax bound to paclitaxel binding sites in cross-linked microtubules in GAB at 37 °C. In the stopped flow device a 2 μM solution of 4-4-20 IgG (*solid line*) or GAB (*dotted line*) was mixed with a solution of 200 nM Hexaflutax and 2 μM sites (final concentrations 1 or 0 μM 4-4-20 IgG) and 100 nM Hexaflutax bound to 1 μM sites (*cyan line*), fitting the data to the sum of three exponentials (*green*, *red*, and *blue lines*). Data were corrected for the observed photobleaching (3%). *Upper inset*, residues between the experimental and the fitting curves (*cyan line* residues to the three-exponential fitting, *orange line* residues to a two-exponential fitting). *Lower inset*, dependence of the observed kinetic rate of the second phase (*red line*) on the concentration of 4-4-20 IgG.

accumulation of beads was observed in open microtubular sheets or at microtubule ends.

Kinetics of Binding of Antibodies to Microtubule-bound Fluorescent Taxoids—To estimate the exposure of the fluorescent moiety of Hexaflutax bound to microtubules to the external solvent, the kinetics of bound ligand fluorescence quenching by the 4-4-20 antibody was measured.

Three phenomena affecting the fluorescence are expected to occur: (*a*) the quenching of the free Hexaflutax (because the affinity of Hexaflutax for its binding site is relatively low, a significant percentage of the Hexaflutax will be free in solution); (*b*) the quenching of the Hexaflutax bound to its site in the microtubules; (*c*) the reshuffling of Hexaflutax/site binding equilibrium because of the difference in affinity between the free Hexaflutax and the antibody-Hexaflutax complex for the site in the microtubules.

To be able to identify the three processes in the quenching curve, appropriate experiments were done to characterize them. First, the kinetic rate of binding of the 4-4-20 antibody to free Hexaflutax was measured (Fig. 4*A*). The free Hexaflutax is quenched very rapidly by the antibody. The velocity of this quenching depends linearly on the concentration of 4-4-20 (Fig. 4*A*, *inset*), which indicates a bimolecular reaction, *i.e.* the binding of the IgG to the fluorescein. The kinetic constant of binding of the antibody to fluorescein can be calculated from the dependence of k_{obs} on the IgG concentration. The value determined for this constant at 37 °C is $1.16 \pm 0.10 \times 10^7$ M^{-1} s^{-1}. Second, the binding affinity of the antibody-Hexaflutax complex for the site in the microtubules at 37 °C was measured and

compared with that of the free Hexaflutax at the same temperature using the centrifugation assay, the values obtained were $7.2 \pm 1.3 \times 10^5$ M^{-1} (free Hexaflutax) and $21.6 \pm 2.3 \times 10^5$ M^{-1} (4-4-20-Hexaflutax).

When mixed in the stopped flow device, the fluorescence of the microtubule-bound Hexaflutax fluorescence is quenched very rapidly by the 4-4-20 antibody. Adequate negative controls with an irrelevant IgG (MOPC 21) showed a fluorescence change similar to that of the buffer (Fig. 4*B*, *dotted line*) within the time range of the experiment, indicating that a slow dissociation of the complex caused by dilution is observed. When the kinetic curves of bound Hexaflutax fluorescence quenching by 4-4-20 (Fig. 4*B*) are analyzed three kinetic phases are observed. (*a*) A very fast initial phase whose rate is linearly dependent on the 4-4-20 concentration, indicating that a bimolecular reaction is observed. The kinetic rate constant determined at 37 °C for this fast phase, which accounts for a 29 ± 8% of the total amplitude, is $1.10 \pm 0.18 \times 10^7$ M^{-1}s^{-1}, coincident with the kinetic rate of quenching of the free antibody; the amplitude (plus the 13% of the fluorescence quenched in within the dead time) coincides with the fraction of free ligand calculated from the binding constant (42%). It is therefore straightforward to assign this initial phase to the quenching of the free ligand. (*b*) A second fast phase whose velocity depends also linearly on the concentration of 4-4-20 (Fig. 4*B*, *inset*), also indicates a bimolecular reaction, *i.e.* the binding of the IgG to the fluorescein of the bound ligand. The kinetic constant of binding of the antibody to fluorescein can be calculated, from the dependence of k_{obs} on the IgG concentration. The value determined for this constant at 37 °C is $2.26 \pm 0.25 \times 10^6$ M^{-1} s^{-1}. (*c*) Finally, a third slow kinetic phase is observed (6 ± 3%) with a rate constant of the order of 0.3 s^{-1}, which is independent of the antibody concentration. Since the amplitude of this phase is negative (is a decrease in fluorescence intensity, as expected from the lower fluorescence of the microtubule-bound 4-4-20-Hexaflutax complex compared with the free 4-4-20-Hexaflutax) and an increase of the percentage of bound antibody-ligand complex should be expected from the binding constants of the Hexaflutax and the 4-4-20 Hexaflutax complex to the site (58% of Hexaflutax bound immediately after dilution and 66% of 4-4-20-Hexaflutax bound at equilibrium), this phase could be assigned to the binding of the excess 4-4-20-Hexaflutax complex to the empty sites. Since the concentration of free 4-4-20-Hexaflutax complex is independent of the free antibody concentration resulting from the high affinity of the antibody for the ligand (essentially all the Hexaflutax is quenched), the observed kinetic rate of this binding was independent of the total 4-4-20 concentration and a pseudo first-order kinetic binding constant of the order of 5×10^6 M^{-1} s^{-1} can be estimated.

The system could be also modeled using the FITSIM package (40) as two simultaneous (the binding of the antibody to the free and bound Hexaflutax) and a consecutive reaction (the binding of the free 4-4-20-Hexaflutax complex to the empty sites), allowing the determination of the kinetic rate constant of binding of the 4-4-20 antibody to the bound Hexaflutax ($2.46 \pm 0.15 \times 10^6$ M^{-1} s^{-1}) for the experiment shown in Fig. 4*B*.

Because the cosedimentation experiments suggest the existence of a transient ternary complex between the antibodies and the Flutax-1 and Flutax-2-microtubule complex, the kinetics of quenching of Flutax-2 by antibodies was measured (Fig. 5). Even if the transient ternary complex is unstable, if the probe is exposed, it might be possible to observe a fast quenching of the fluorescence, which will indicate binding of the antibody to the microtubule-Flutax-2 complex. Because the short linker of Flutax-1 and Flutax-2 interferes with the binding of the 4-4-20 antibody to their fluorescent moiety, resulting in a lower percentage of quenching and a low affinity, we then employed the polyclonal IgG. When mixed in the stopped flow device, 90% of the Flutax-2 fluorescence is quenched very rapidly, following an exponential decay with an observed rate constant that linearly depends on the concentration of IgG (Fig. 5*A*, *inset*). Adequate controls with nonimmune rabbit IgG were performed. The value determined for the binding rate constant at 37 °C is $3.03 \pm 0.10 \times 10^6$ M^{-1} s^{-1}. After the first fast phase, a slow decay of the fluorescence intensity of the sample can be observed (Fig. 5*B*, *solid line*). The kinetics of this second phase is not dependent on the concentration of IgG, indicating a monomolecular reaction. The kinetic constant of this step at 37 °C is $1.74 \pm 0.20 \times 10^{-2}$ s^{-1}, very similar to the kinetic rate of dissociation of Flutax-2, $1.92 \pm 0.10 \times 10^{-2}$ s^{-1} (11), suggesting that this second step may correspond to the dissociation of the antibody-Flutax-2 complex from microtubules (sedimentation experiments confirmed that Flutax-1 and Flutax-2 dissociate from microtubules after binding to polyclonal and 4-4-20 monoclonal antibodies (see "Materials and Methods"). Since Flutax-2 dissociation from microtubules does not significantly change its fluorescence intensity, the kinetics of dissociation of Flutax-1 from microtubules in the same conditions, whose kinetic rate ($k = 1.79 \pm 0.07 \times 10^{-2}$ s^{-1}) is almost

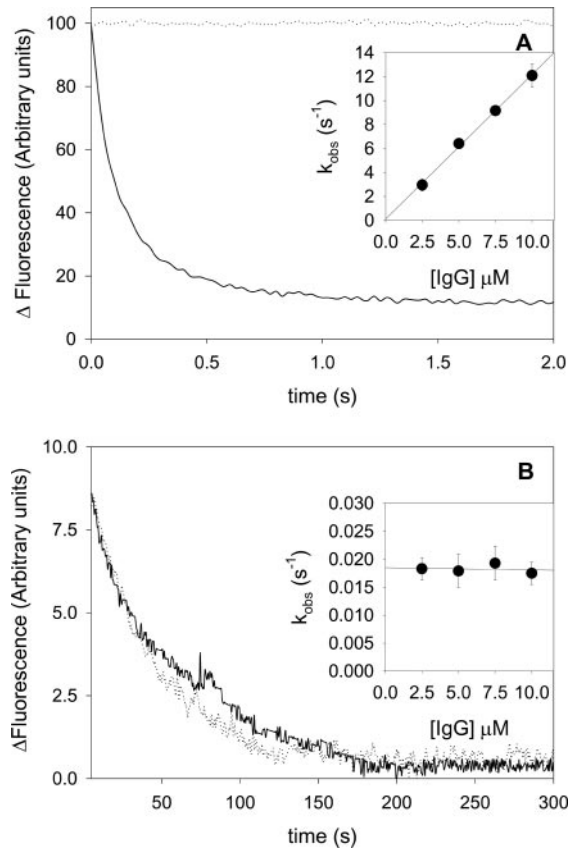

FIG. 5. *A*, *solid line*, kinetics of binding at 37 °C (from 0 to 2 s) of 10 μM antifluorescein IgG to 100 nM Flutax-2 bound to 1 μM paclitaxel binding sites in cross-linked microtubules in GAB (a control was performed to check that essentially all of the Flutax-2 was specifically bound to the microtubules). *Dotted line*, kinetics of binding at 37 °C (from 0 to 2 s) of 10 μM nonimmune IgG to 100 nM Flutax-2 bound to 1 μM paclitaxel binding sites in cross-linked microtubules in GAB. *Inset*, dependence of the observed kinetic rate on the active concentration of IgG. *B*, *solid line*, continuation of the kinetics of binding at 37 °C (from 2 to 300 s) of 10 μM antifluorescein IgG to 100 nM Flutax-2 bound to 1 μM paclitaxel binding sites in cross-linked microtubules in GAB. *Dotted line*, kinetics of displacement of Flutax-1 bound to 1 μM paclitaxel binding sites in cross-linked microtubules by 100 μM docetaxel. *Inset*, dependence of the observed kinetic rate on the concentration of IgG.

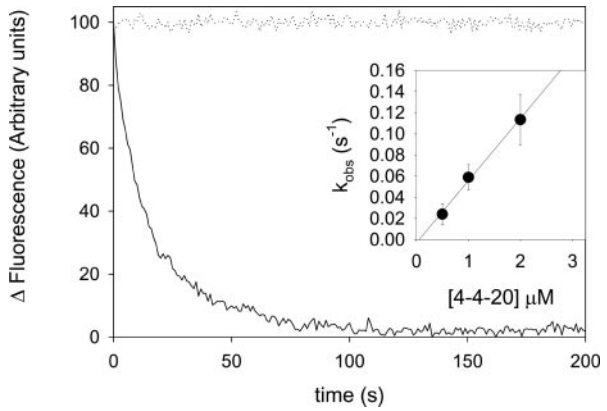

FIG. 6. *Solid line*, kinetics of binding at 37 °C of 1 μM 4-4-20 IgG to 200 nM Hexaflutax bound to 20 μM paclitaxel binding sites in MAP-stabilized microtubules in AB (a control was performed to check that essentially all of the Hexaflutax was specifically bound to the microtubules). *Dotted line*, kinetics of binding at 37 °C of 1 μM MOPC 21 IgG to 200 nM Hexaflutax bound to 20 μM paclitaxel binding sites in MAP-stabilized microtubules in AB. Data were corrected for the observed photobleaching (5%). *Inset*, dependence of the observed kinetic rate on the concentration of IgG.

identical to that of Flutax-2 (11), is shown for comparison purposes (Fig. 5*B*, *dotted line*).

It is interesting to point out that for the different antibody-fluorescein complexes with Flutax-2 and Hexaflutax the kinetic rate of binding is very similar in both cases ($2–3 \times 10^6$ M^{-1} s^{-1}). This indicates that the same kinetic step should limit the binding reaction. The diffusion limit for the binding of a large molecule like an antibody (approximately 60 Å R_g) to a large rod like a microtubule (11) should be of the order of 10^7 M^{-1} s^{-1} at 37 °C. Since the determined association rates are close to these limit and they are very similar, it is reasonable to propose that the quenching reactions are diffusion-controlled, which indicates a similar exposition of the epitope, *i.e.* the fluorescein, independently of the linker.

To confirm that cross-linking is not affecting the accessibility of the antibodies to Hexaflutax and Flutax-2, controls were done with noncross-linked microtubules. In those microtubules the ligands are added to dimeric tubulin prior to assembly, the association rate constants measured being similar to those observed using cross-linked ones.

Kinetics of Binding of Antibodies to Bound Hexaflutax in the Presence of MAPs—To determine whether surface-bound MAPs affect the accessibility of bound Hexaflutax, kinetic studies were performed using microtubules stabilized by MAPs instead of cross-linked microtubules. Fig. 6 shows the time course of binding of 4-4-20 antibody to microtubules assembled from microtubular protein in AB. It can be noticed that the quenching is much slower than that of Hexaflutax bound to cross-linked microtubules. The kinetics is linearly dependent on the antibody concentration, indicating a bimolecular reaction. The kinetic rate constant measured at 37 °C was $5.9 \pm 0.1 \times 10^4$ M^{-1} s^{-1}, which is 40 times slower than that observed for cross-linked microtubules in GAB. Additionally, since the observed kinetic rates of Hexaflutax quenching in our experimental conditions (Fig. 6) are of the same order of magnitude as the dissociation rate constant of Hexaflutax at 37 °C ($10.7 \pm 0.2 \times 10^{-2}$ s^{-1}),[2] a necessary sedimentation control was performed. Essentially all Hexaflutax remains specifically bound to microtubules after quenching (it dissociates after the addition of an excess of docetaxel). Adequate controls were also performed to discard any effects caused by the buffer composition.

[2] J. F. Díaz and A. García-Carril, unpublished results.

Binding of Antibodies to Fluorescent Taxoids in Microtubule Cytoskeletons—To check the accessibility of the antibodies to the probes in a more physiological situation, the kinetics of quenching of the fluorescence of ligands bound to native cytoskeletons from PtK2 cells at 25 °C has been semiquantitatively characterized approaching pseudo first-order conditions, employing CCD-detected epifluorescence microscopy images (Fig. 7). The plot of the averaged fluorescence intensity *versus* time shows an exponential partial decay of the fluorescence, the kinetics of the reaction being dependent on the concentration of antibody, which indicates a bimolecular reaction.

The half-life of the quenching process of Hexaflutax at 25 °C by 1 μM 4-4-20 monoclonal antibody is 60 s ($k_{obs} = 8.5 \times 10^{-3}$ s^{-1}), which corresponds to a value of $k_+ = 8.5 \times 10^3$ M^{-1} s^{-1}, 250 times slower than that of quenching of Hexaflutax bound to *in vitro* microtubules assembled from pure tubulin and 7 times slower than the quenching of Hexaflutax bound to microtubules assembled from microtubular protein, although the latter value has been obtained at 37 °C, which may explain the difference observed.

The accessibility of the bound Flutax-1 and Flutax-2 to antibodies was studied using the same polyclonal antibody employed previously. At 1 μM and 25 μM total antibody concentration (200 nM and 5 μM antifluorescein antibody concentration) the process is very slow compared with the fast quenching observed with *in vitro* assembled microtubules (k_{obs} approximately 10^{-3} s^{-1}) and independent of the antibody concentration, which discards a bimolecular reaction, suggesting that Flutax-1 and Flutax-2 are fully protected by the cytoskeletal MAPs and that the observed slow quenching is simply the result of dissociation of the ligands from the site.

Molecular Modeling—To visualize the accessibility of the fluorescent moiety of Hexaflutax bound to microtubules to a large molecule like an antibody, the ligand-microtubule complex has been modeled with the paclitaxel moiety bound to the luminal site (Fig. 8*A*). In the modeled complex the fluorescein moiety lies in between the protofilaments, not being accessible to the antibody. To show the inaccessibility, the ternary complex between 4-4-20, Hexaflutax, and microtubules has been modeled as well (Fig. 8*B*). Because no complete structure of the IgG is available, the structure of the Fab fragment (4FAB (43, 44)) was used. The modeling shows that in the best possible conformation of the hexanoyl linker, the antibody would have to interpenetrate the tubulin to bind to the fluorescein moiety of the bound Hexaflutax.

DISCUSSION

The taxoid binding site in microtubules has recently been found to be the target of many chemically different drugs (microtubule-stabilizing agents). The location and nature of the taxoid binding site in microtubules have been the objects of intensive research in the last years. The site was initially mapped in the interprotofilament space (9), a location that would be compatible with the observed facts that it stabilizes the lateral interaction between protofilaments, alters the angle of contact between them, and the binding site only exists in microtubules and not in the soluble dimer (8, 9, 45–47). But later, the high resolution model of microtubules, obtained by fitting the protofilament structure from electron crystallography of Zn^{2+}-induced tubulin sheets, placed the binding site in the lumen of the microtubules (20). This location of the binding site does not offer a straightforward explanation to the fact that the binding site exists only in the assembled tubulin. Additionally, such a location of the binding site would be relatively restrictive for the binding of paclitaxel to preassembled microtubules. Studies with fluorescent labeled ligands have shown that Flutax-1, Flutax-2, and Paclitaxel bind rapidly to micro-

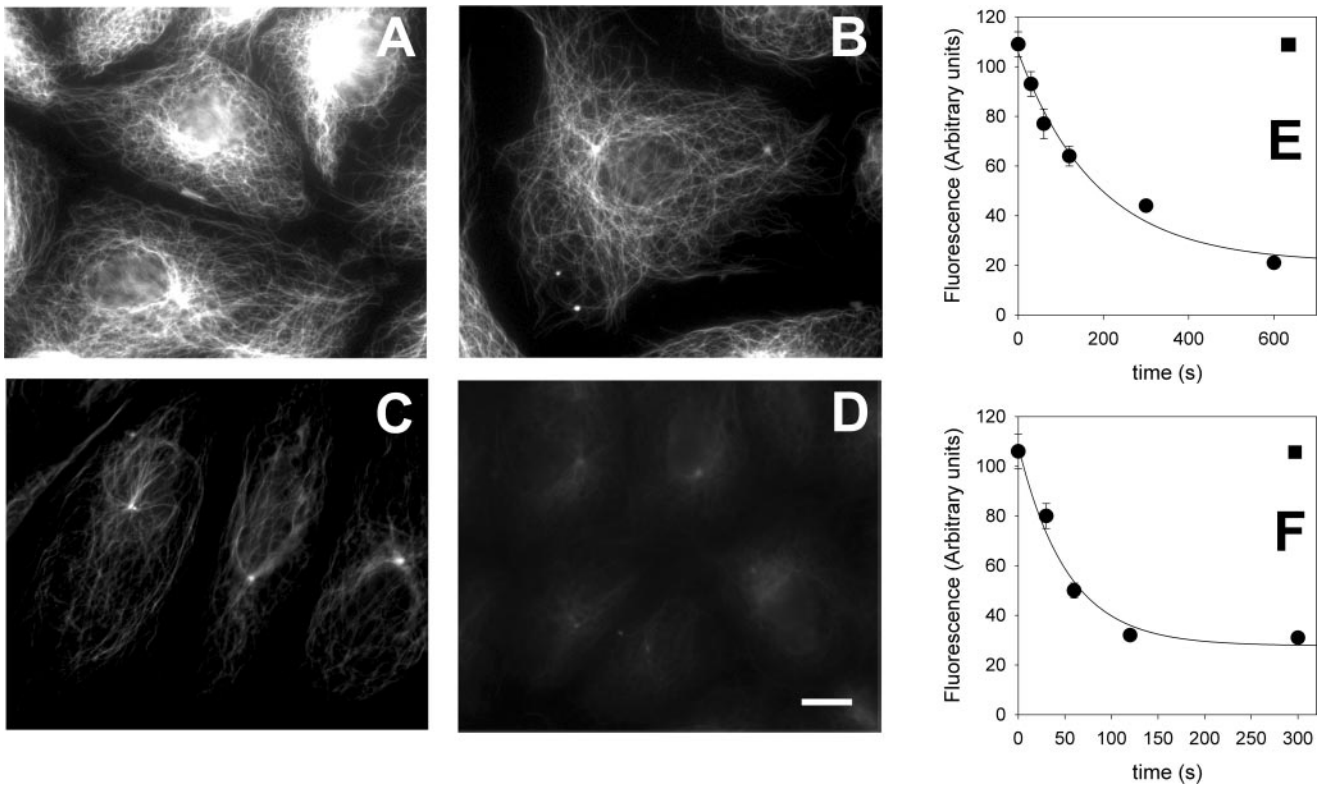

FIG. 7. **Representative images of kinetics of 4-4-20 quenching of fluorescence of Hexaflutax bound to cytoskeletons from PtK2 interphase cells (*A–D*).** *A*, 0-s incubation in 1 μM 4-4-20; *B*, 1-min incubation in 1 μM 4-4-20; *C*, 2-min incubation in 1 μM 4-4-20; *D*, 5-min incubation in 1 μM 4-4-20. The *bar* represents 10 μm. *E*, time course of averaged fluorescence intensity of cytoskeletons of interphase Ptk2 cells after incubation with 200 nM 4-4-20. The *solid line* is the best fitting to a single exponential curve, the *square* represents the average fluorescence of the controls incubated with PEMP only. *F*, time course of the averaged fluorescence intensity of cytoskeletons of interphase Ptk2 cells after incubation with 1 μM 4-4-20. The *solid line* is the best fitting to a single exponential curve, the *square* represents the average fluorescence of the controls incubated with PEMP only.

tubules assembled from pure tubulin, both cross-linked and native, to microtubules assembled from microtubular protein and to native cellular cytoskeletons (10–12). Although it has been suggested that the ligand may pass through pores or openings (20), the size of any realistic pore in the microtubule wall is too small for the ligand to diffuse passively toward the lumen of the microtubule, and large openings would result in kinetic inhomogeneity of the samples, which has not been observed (11, 12).

To potentially reconcile the kinetic binding results with the model structure of microtubules an alternative mechanism of binding has been proposed in which the taxoid site ligands bind to an external site at the microtubule pores, this being followed by a conformational change that facilitates ligand transport to the final luminal site (12). The conformational change would move some of the residues of the binding site toward the lumen, canceling the outer binding site and creating the new inner binding site. In such a way the observed binding stoichiometry would be 1:1, and the sites would not exist in the unassembled tubulin because the inner site would not be complete, and the outer site would require the interprotofilament contact to be completed.

The Fluorescein Moiety of Fluorescent Taxoids Is Accessible to Antibodies—The accessibility of bound ligands to the solvent was tested by measuring the binding of a large molecule like an IgG to the prebound ligand. IgG molecules (R_g 6 nm; 48) can hardly diffuse into the microtubule lumen (7.5 nm radius) through any possible fenestration in the microtubule wall. Diffusion from the microtubule ends would be impossible because the first molecule to bind would block the way. Modeling Flutax or Hexaflutax in the luminal site in the most exposed configuration (Fig. 8) results in a configuration that is unreachable for an IgG, so any significant ternary complex detected has to have the ligand probe bound to an outer site.

The ternary complex antibody-microtubule-Hexaflutax can be detected both by SDS-PAGE of cross-linked and noncross-linked microtubules and by the use of a gold-labeled secondary antibody. Because it is not possible for the antibody to enter the microtubules through any realistic fenestration, the existence of the ternary complex demonstrates the existence of an outer binding site for Hexaflutax, a *bona fide* fluorescent analog of paclitaxel, which is displaced from this binding site by docetaxel (Fig. 2, *Gel 1*, *lane C*; *Gel 3*, *lane D*, and Fig. 3*B*) and paclitaxel (not shown). The results indicate that this site is shared with paclitaxel, supporting the hypothesis of the paclitaxel outer binding site.

After confirming the existence of the outer paclitaxel binding site we wanted to know how much of the fluorescent ligand is bound to this external binding site and how much would be in the luminal site, to know the relevance of this external binding site in the final microtubule structure. To do so, it was necessary to know how much of the ligand bound is immediately accessible to the antibody. Even if only a fraction of the fluorescein moieties were exposed to the solvent they would be immediately bound by the antibody, and this binding would shift the equilibrium of internalization toward the outer site, resulting in the formation of the ternary complex, microtubule-ligand-antibody that has been trapped by centrifugation techniques. The centrifugation technique does not allow us to discriminate how much of the ligand bound is immediately accessible to the antibody because of the long dead time. The quenching kinetics was measured to check whether the anti-

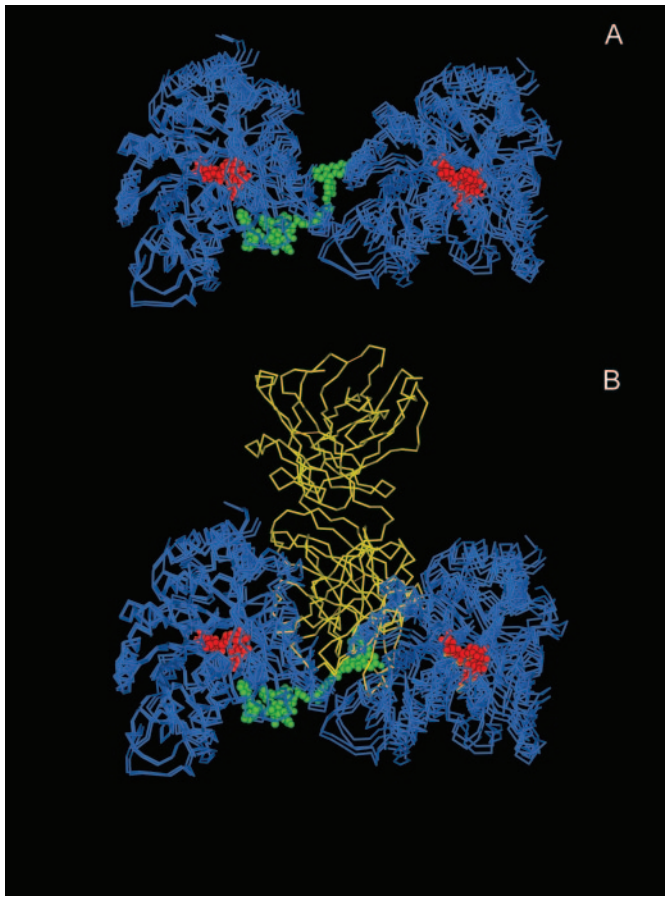

FIG. 8. *A*, model of Hexaflutax-microtubule complex. The conformation of the linker between the fluorescein and the paclitaxel moiety has been modified to maximize the exposure of the fluorescein to the solvent. *B*, model of 4-4-20-Hexaflutax-microtubule complex. The conformation of the linker between the fluorescein and the paclitaxel moiety has been modified to minimize the steric conflict between the Fab and tubulin. *Green beads*, Hexaflutax bound at the paclitaxel site; *red beads*, nucleotide bound at its site.

body binds initially to a small fraction of the ligand in the outer site, displacing the internalization equilibrium toward the external site, or whether all of the ligand is exposed to the antibody. When the antibody is mixed with the Hexaflutax-microtubule complex the fluorescence intensity change is completed very rapidly (80% of the fluorescence is quenched as for the free Hexaflutax), indicating that there is no restriction for the antibody to access all the binding sites. The reaction has an observed kinetic rate linearly dependent on the concentration of antibody, which indicates a bimolecular reaction between the fluorescent moiety of the ligand and the antibody. It might be argued that the detailed kinetics of the Hexaflutax-microtubule interaction is unknown, so it is not known whether there is the putative internalization kinetic step observed for Flutax-1 and Flutax-2 (11). In this way the result (Hexaflutax is mainly bound to an external site) cannot be extrapolated to the other fluorescent taxoids. To do so, a similar kinetic experiment was performed using a polyclonal antibody against fluorescein and Flutax-2 as bound ligand. The observed kinetics was fast as well, of the same order of magnitude as that of Hexaflutax, the quenching of the fluorescence was almost complete (90%), and the kinetics of the reaction was dependent on the antibody concentration, indicating that Flutax-2 is also bound mainly to an external site. After quenching, a second kinetic small phase whose rates are coincident with the dissociation of Flutax-2 from its site was observed, indicating that the binding of antibody to the fluorescent probe perturbs the paclitaxel-site interaction. The result implies that the second monomolecular reaction observed previously for Flutax-1 and Flutax-2 binding (11) cannot be assigned to an internalization process and should correspond to a weak binding of the fluorescent moiety.

Protection of the Fluorescent Probe by MAPs—If Hexaflutax fluorescent moieties are exposed in the outer part of the microtubule, it is reasonable to think that the presence of MAPs, which bind to the outer side of the microtubules, should protect them from antibodies. The quenching kinetics of Hexaflutax bound to MAP-containing microtubules is much slower than that of Hexaflutax bound to microtubules assembled from pure tubulin, indicating protection of the bound Hexaflutax.

The protection has been checked as well by following the time course of quenching of ligands bound to native cytoskeletons of PtK2 cells. The kinetics of quenching of Hexaflutax bound to the cytoskeletons is compatible with the quenching of the ligand bound to MAP-containing microtubules, indicating that the binding site is similar both in the reconstituted and the stabilized microtubules and that the presence of cytoskeletal MAPs partially protects Hexaflutax from the antibody. When the same experiment is performed with Flutax-1 or Flutax-2 bound to the site and polyclonal antibody, the ligand is fully protected by the cytoskeletal MAPs.

Fluorescent Taxoids Bind to an External Binding Site That Is Shared with Paclitaxel—The above results indicate that the fluorescent taxoids are bound mainly to an external site. Because it is not possible for the antibody to enter the lumen of the microtubule through any reasonable pores or possible defects in the microtubule wall, and diffusion from the ends would be severely restricted, the fluorescent moiety of the ligands should be necessarily exposed to the outer solvent. The molecular models have shown that it is not possible to expose the fluorescein moieties completely to the outer solvent, while the paclitaxel moiety is bound to its site in the microtubule lumen. It is also known (10, 11, 31, 42, 49–51) that paclitaxel and the fluorescent taxoids compete for the same site with mutual exclusive binding.

Therefore we propose that paclitaxel, Flutax-2, and Hexaflutax bind to an external site on the microtubule surface in the type 1 pores (see Fig. 9 in Ref. 12). Such location of a microtubule assembly inducer would not be unique because doublecortin, a MAP, binds, covering the microtubule pores and inducing tubulin assembly (52). Transport of paclitaxel through the pores to the luminal site may be a subsequent step of binding to this final location (although we cannot say from our data whether paclitaxel itself is internalized to the luminal site derived from structural studies on Zn-sheets (20)), which is restricted in the case of the fluorescent taxoids. Such a mechanism, while keeping the final paclitaxel binding site in the lumen of the microtubule, will justify (*a*) the easy accessibility of taxoids to their binding site, (*b*) the absence of the binding site in the nonassembled microtubules, and (*c*) the influence of taxoid binding in the microtubule protofilament number.

It is known that fluorescent taxoids are able to induce microtubule polymerization (10), so binding at the outer (Flutax) or inner (paclitaxel) site induces assembly. Binding to the luminal site is then obviously not necessary to induce microtubule assembly, indicating that the proposed ligand-induced conformational change (20, 22, 53–55) is not required to justify microtubule assembly induction, and suggesting a preferential binding mechanism (the assembly equilibrium is displaced toward the assembled microtubules because of the higher affinity of the ligand for the microtubules than for the soluble dimer).

Implications of the Existence of an External Paclitaxel Binding Site—A relative large number of compounds with microtu-

bule stabilizing activity (microtubule-stabilizing agents) have been discovered. The compounds whose activity has been confirmed can be divided into two different groups, those that bind to the paclitaxel site (paclitaxel and its analogs, epothilones, eleuterobins, sarcodyctins, discodermolide, 3,17-diacetoxy-2ethoxy-6oxo-B-homo-estra-1,3,5 (10)-triene) (49, 50, 56–58), and those that share the laulimalide site (laulimalide and peloruside) (49, 59).

The compounds that bind to the paclitaxel site are very different from a chemical point of view, although all of them are hydrophobic. If the proposed outer site is just a hydrophobic pocket, it will hold, with lower or higher affinity, a large number of different chemical structures. Some of them (paclitaxel) will induce a conformational change and will be transported to the internal site, whereas others (Hexaflutax, and Flutax-2), which have a negatively charged moiety that may interact with the positively charged residues of the upper part of the pore (12), will not be able to internalize. The assembly induction would be caused by preferential binding, so all of the ligands would have the same effect independently of having a final external or luminal binding site.

It is not known which of the ligands that compete with paclitaxel bind to the inner or outer site, but any ligand that binds to the paclitaxel site in assembled microtubules, including paclitaxel itself, would have to bind to the outer site first (otherwise binding would be extremely slow), then it could stay there or be internalized to the luminal site. Therefore, the outer site should be of great importance for antitumor drug design.

Acknowledgments—We thank Prof. Edward W. Voss Jr. (University of Illinois at Urbana-Champaign) who provided antifluorescein rabbit polyclonal IgG and antifluorescein mouse monoclonal IgG 4-4-20, Mariana Arce for the preparation of the fluorescent taxoids, and Dr. Consuelo López and the late Dr. José Laynez for the use of the stopped flow apparatus. We also thank Matadero Madrid Norte S.A. and José Luis Gancedo S.L. for providing the calf brains for tubulin purification.

REFERENCES

1. Schiff, P. B., Fant, J., and Horwitz, S. B. (1979) *Nature* **277,** 665–667
2. Schiff, P. B., and Horwitz, S. B. (1980) *Proc. Natl. Acad. Sci. U. S. A.* **77,** 1561–1565
3. Bollag, D. M., McQueney, P. A., Zhu, J., Hensens, O., Koupal, L., Liesch, J., Goetz, M., Lazarides, E., and Woods, C.M. (1995) *Cancer Res.* **55,** 2325–2333
4. Wani, M. C., Taylor, H. L., Wall, M. E., Coggon, P., and McPhail, A. T. (1971) *J. Am. Chem. Soc.* **93,** 2325–2327
5. Ter Haar, E., Kowalski, R. J., Hamel, E., Lin, C. M., Longley, R. E., Gunasekera, S. P., Rosenkranz, H. S., and Day, B. W. (1996) *Biochemistry* **35,** 243–250
6. Long, B. H., Carboni, J. M., Wasserman, A. J., Cornell, L. A., Casazza, A. M., Jensen, P. R., Lindel, T., Fenical, W., and Fairchild, C. R. (1998) *Cancer Res.* **58,** 1111–1115
7. Choy, H. (2001) *Crit. Rev. Oncol. Hematol.* **37,** 237–247
8. Andreu, J. M., Bordas, J., Díaz, J. F., García de Ancos, J., Gil, R., Medrano, F. J., Nogales, E., Pantos, E., and Towns-Andrews, E. (1992) *J. Mol. Biol.* **226,** 169–184
9. Nogales, E., Wolf, S. G., Khan, I. A., Ludueña, R. F., and Downing, K. H. (1995) *Nature* **375,** 424–427
10. Evangelio, J. A., Abal, M., Barasoain, I., Souto, A. A., Acuña, A. U., Amat-Guerri, F., and Andreu, J. M. (1998) *Cell Motil. Cytoskeleton* **39,** 73–90
11. Díaz, J. F., Strobe, R., Engelborghs, Y., Souto, A. A., and Andreu, J. M. (2000) *J. Biol. Chem.* **275,** 26265–26276
12. Díaz, J. F., Barasoain, I., and Andreu, J. M. (2003) *J. Biol. Chem.* **278,** 8407–8419
13. Díaz, J. F., Menéndez, M., and Andreu, J. M. (1993) *Biochemistry* **32,** 10067–10077
14. Nogales, E., Wolf, S. G., and Downing, K. (1998) *Nature* **391,** 199–203
15. Larsson, H., Wallin, M., and Edstrom, A. (1976) *Exp. Cell Res.* **100,** 104–110
16. Mandelkow, E. M., Schulteiss, R., Rapp, R., Müller, M., and Mandelkow, E. (1986) *J. Cell Biol.* **102,** 1067–1073
17. Wade, R. H., Chrétien, D., and Job, D. (1990) *J. Mol. Biol.* **212,** 775–786
18. Sosa, H., Dias, D. P., Hoenger, A., Whittaker, M., Wilson-Kubalek, E., Sablin, E., Fletterick, R. J., Vale, R. D., and Milligan, R.A. (1997) *Cell* **90,** 217–224
19. Meurer-Grob, P., Kasparian, J., and Wade, R. H. (2001) *Biochemistry* **40,** 8000–8008
20. Nogales, E., Whittaker, M., Milligan, R. A., and Downing, K. H. (1999) *Cell* **96,** 79–88
21. Chacón, P., and Wriggers, W. (2002) *J. Mol. Biol.* **317,** 375–384
22. Li, H., DeRosier, D. J., Nicholson, W. V., Nogales, E., and Downing, K.H. (2002) *Structure* (*Lond.*) **10,** 1317–1328
23. Rao, S., Horwitz, S. B., and Ringel, I. (1992) *J. Natl. Cancer Inst.* **84,** 785–788
24. Rao, S., Krauss, N. E., Heerding, J. M., Swindell, C. S., Ringel, I., Orr, G. A., and Horwi, S. B. (1994) *J. Biol. Chem.* **269,** 3132–3134
25. Rao, S., Orr, G. A., Chaudhary, A. G., Kingston, D. G., and Horwitz, S. B. (1995) *J. Biol. Chem.* **270,** 20235–20238
26. Giannakakou, P., Sackett, D. L., Kang, Y. K., Zhan, Z., Buters, J. T., Fojo, T., and Poruchynsky, M. S. (1997) *J. Biol. Chem.* **272,** 17118–17125
27. Gonzalez-Garay, M. L., Chang, L., Blade, K., Menick, D. R., and Cabral, F. (1999) *J. Biol. Chem.* **274,** 23875–23882
28. Rao, S., He, L., Chatkravarty, S., Ojima, I., Orr, G. A., and Horwitz, S. B. (1999) *J. Biol. Chem.* **274,** 37990–37994
29. Díaz, J. F., and Andreu, J. M. (1993) *Biochemistry* **32,** 2747–2755
30. de Pereda, J. M., Wallin, M., Billger, M., and Andreu, J. M. (1995) *Cell Motil. Cytoskeleton* **30,** 153–163
31. Andreu, J. M., and Barasoain, I. (2001) *Biochemistry* **40,** 11975–11984
32. Souto, A. A., Acuña, A. U., Andreu, J. M., Barasoain, I., Abal, M. Y, and Amat-Guerri, F. (1995) *Angew. Chem. Int. Ed. Eng.* **34,** 2710–2712
33. Kranz, D. M., and Voss, E. W., Jr. (1981) *Mol. Immunol.* **18,** 889–898
34. Arevalo, M. A., Nieto, J. M., Andreu, D., and Andreu, J. M. (1990) *J. Mol. Biol.* **214,** 105–120
35. De Inés, C. (1995) *Interaction of Cellular Microtubules with Specific Antibodies and New Antitumoral Compounds*, Ph.D. thesis, pp. 59–92, Universidad Complutense de Madrid
36. Chan, M. F., Radeke, M. J., de Inés, C., Barasoain, I., Kohlstaedt, L. A., and Feinstein, S. C. (1998) *Biochemistry* **37,** 17692–17703
37. Modig, C., Olsson, P. E., Barasoain, I., de Inés, C., Andreu, J. M., Roach, M. C., Ludueña, R. F., and Wallin, M. (1999) *Cell Motil. Cytoskeleton* **42,** 315–330
38. Lackowicz, J. R. (1999) *Principles of Fluorescence Spectroscopy*, 2nd Ed., pp. 291–318, Kluwer Academic, New York
39. Bevington, P. R. (1969) *Data Reduction and Error Analysis for the Physical Sciences*, pp. 235–240, McGraw-Hill Book Co., New York
40. Barshop, B. A., Wrenn, R. F., and Frieden, C. (1983) *Anal. Biochem.* **130,** 134–145
41. de Inés, C., Leynadier, D., Barasoain, I., Peyrot, V., Garcia, P., Briand, C., Rener, G. A., and Temple, C., Jr., (1994) *Cancer Res.* **54,** 75–84
42. Abal, M., Souto, A. A., Amat-Guerri, F., Acuña, A. U., Andreu, J. M., and Barasoain, I. (2001) *Cell. Motil. Cytoskeleton* **49,** 1–15
43. Whitlow, M., Howard, A. J., Wood, J. F., Voss, E. W., Jr., and Hardman, K. D. (1995) *Protein Eng.* **8,** 749–761
44. Herron, J. N., He, X. M., Mason, M. L., Voss, E. W., and Edmundson, A. B. (1989) *Proteins* **5,** 271–280
45. Andreu, J. M., Díaz, J. F., Gil, R., de Pereda, J. M., García de Lacoba, M., Peyrot, V., Briand, C., Towns-Andrews, E., and Bordas, J. (1994) *J. Biol. Chem.* **269,** 31785–31792
46. Díaz, J. F., Andreu, J. M., Diakun, G., Towns-Andrews, E., and Bordas, J. (1996) *Biophys. J.* **70,** 2408–2420
47. Díaz, J. F., Valpuesta, J. M., Chacon, P., Diakun, G., and Andreu, J. M. (1998) *J. Biol. Chem.* **273,** 33803–33810
48. Kilar, F., Simon, I., Lakatos, S., Vonderviszt, F., Medgyesi, G. A., and Zavodszky, P. (1985) *Eur. J. Biochem.* **147,** 17–25
49. Pryor, D. E., O'Brate, A., Bilcer, G., Díaz, J. F., Wang, Y., Wang, Y., Kabaki, M., Jung, M. K., Andreu, J. M., Gosh, A. K., Giannakakou, P., and Hamel, E. (2002) *Biochemistry* **41,** 9109–9115
50. Nicolaou, K. C., Ritzén, A., Namoto, K., Buey, R. M., Díaz, J. F., Andreu, J. M., Wartmann, M., Altmann, K. H., O'Brate, A., and Giannakakou, P. (2002) *Tetrahedron* **58,** 6413–6432
51. Buey, R. M., Díaz, J. M., Andreu, J. M., O'Brate, A., Giannakakou, P., Nicolaou, K. C., Sasmal, P., Ritzén, A., and Namoto, K. (2004) *Chem. Biol.* **11,** 225–236
52. Moore, C. A., Perderiset, M., Francis, F., Chelly, J., Houdusse, A., and Milligan, R. A. (2004) *Mol. Cell* **14,** 833–839
53. Amos, L. A., and Lowe, J. (1999) *Chem Biol.* **6,** R65–R69
54. Downing, K. H. (2000) *Annu. Rev. Cell Dev. Biol.* **16,** 89–111
55. Snyder, J. P., Nettles, J. H., Cornett, B., Downing, K. H., and Nogales, E. (2001) *Proc. Natl. Acad. Sci. U. S. A.* **98,** 5312–5316
56. Hamel, E., Sackett, D. L., Vourloumis, D., and Nicolaou, K. C. (1999) *Biochemistry* **38,** 5490–5498
57. Hung, D. T., Chen, J., and Schreiber, S. L. (1996) *Chem. Biol.* **3,** 287–293
58. Jiménez-Barbero, J., Amat-Guerri, F., and Snyder, J. P. (2002) *Curr. Med. Chem., Anticancer Agents* **2,** 91–122
59. Gaitanos, T., Buey, R. M., Díaz, J. F., Northcote, P. T., Teesdale-Spittle, P., Andreu, J. M., and Miller, J. H. (2004) *Cancer Res.* **64,** 5063–5067